The Astrophysical Journal Letters, 925:L19 (8pp), 2022 February 1 https://doi.org/10.3847/2041-8213/ac4d8e

TeV and keV–MeV Excesses as Probes for Hadronic Process in BL Lacertaes

Ji-Gui Cheng[1], Xiao-Li Huang[2], Ze-Rui Wang[3], Jian-Kun Huang[1], and En-Wei Liang[1]
[1] Guangxi Key Laboratory for Relativistic Astrophysics, School of Physical Science and Technology, Guangxi University, Nanning 530004, People's Republic of China; lew@gxu.edu.cn
[2] Guizhou Provincial Key Laboratory of Radio Astronomy and Data Processing, School of Physics and Electronic Science, Guizhou Normal University, Guiyang 550025, People's Republic of China xiaoli.huang@gznu.edu.cn
[3] College of Physics and Electronic Engineering, Qilu Normal University, Jinan 250200, People's Republic of China
Received 2021 November 21; revised 2022 January 18; accepted 2022 January 20; published 2022 February 2

Abstract

A hard TeV γ-ray component excess over the single-zone leptonic model prediction (TeV excess) is observed in the spectral energy distributions (SEDs) of some BL Lacs. Its origin is uncertain. We revisit this issue with four BL Lacs (1ES 0229+200, 1ES 0347–121, 1ES 1101–232, and H2356–309), in which the TeV excess is detected in their intrinsic SEDs. We represent their SEDs with a single-zone leptohadronic model, where radiations of the electrons and protons as well as the cascade electrons produced by the $\gamma\gamma$ and pγ interactions within their jets are considered. We show that the observed SEDs below the GeV gamma-ray band are attributed to the synchrotron radiations and self-Compton process of the primary electrons, and the TeV excess is explained with the γ-ray emission from the pγ process via the π^0 decay. The cascade emission of the electrons produced via the $\gamma\gamma$ and pγ interactions results in a keV–MeV excess in the SEDs, illustrated as a bump or plateau. This extra photon field enhances the production of TeV photons from the $p\gamma$ process, resulting in a reduction of the proton power by about one order of magnitude. However, the derived powers are still 3–4 orders of magnitude larger than the Eddington limit, being challenged by the current black hole accretion physics. Applying our model to Mrk 421, we propose that synergic observations with current and upcoming TeV and keV–MeV telescopes for its tentative TeV and MeV excesses can give insights to the hadronic process in its jet.

Unified Astronomy Thesaurus concepts: Blazars (164); Relativistic jets (1390); Non-thermal radiation sources (1119)

1. Introduction

Most TeV γ-ray-emitting active galactic nuclei (AGNs) are BL Lacertaes (BL Lacs).[4] Their observed broadband spectral energy distributions (SEDs) are characterized as bimodal distributions with peaks at the IR–optical–X-ray and the MeV–GeV bands (Urry & Padovani 1995). The SEDs generally are attributed to leptonic processes of relativistic electrons accelerated within the jets. The peak at the low-energy band is explained as synchrotron radiation of the electrons, and the high-energy peak results from the synchrotron self-Compton (SSC) scattering process (e.g., Maraschi et al. 1992; Ghisellini & Madau 1996). Zhang et al. (2012) presented a systematic analysis for the SEDs of 24 TeV BL Lacs with the single-zone leptonic model. They showed that most SEDs are indeed well represented with the model.

TeV-selected BL Lacs are the most valuable sources for studying particle accelerations and radiation physics. The obstacle for this purpose is that the extragalactic TeV photons are absorbed by the extragalactic background light (EBL) via the pair production process when traveling through the universe (Gould & Schréder 1966). Interestingly, the intrinsic SEDs of some BL Lacs show an apparent excess in the TeV band (the TeV excess) by correcting the EBL absorption. The excess is an extra hard spectral component that is difficult to explain with the single-zone leptonic model. For instance, High-Energy Stereoscopic System (HESS) observations show that the intrinsic photon spectrum in an outburst of 1ES 1101–232 during 2004 March–2005 June is very hard with a power-law index $\sim$1.5 in the energy range from 0.23 to 4 TeV (Aharonian et al. 2007a). In the hadronic model, the TeV excess is suggested to be produced through proton–synchrotron radiation or the decay of neutral pions produced via the *pp* or $p\gamma$ interaction process (Mannheim 1993). Cao & Wang (2014) studied the possible hadronic origin of the hard γ-ray spectrum and suggested that the TeV excess would originate from the decay of neutral pions produced through pγ interactions in which the soft photons are from electron synchrotron radiation within the jet. Sahu et al. (2013) proposed that the observed TeV orphan flare of 1ES 1959+650 is also from the photohadronic process. Mastichiadis et al. (2013) investigated the X-ray and γ-ray variabilities of Mrk 421 in various leptohadronic scenarios and found that the hadronic model can reproduce the quadratic behavior between X-ray and TeV observations. Alternatively, it has been found that the TeV excess could originate from leptonic processes of different radiation zones such as inverse Compton scattering of cosmic microwave background (IC/CMB) photons by electrons in the large-scale jet (Böttcher et al. 2008; Yan et al. 2012) or an SSC process in a more distant region away from the emitting region that is responsible for the outbursts in the keV–GeV band (Zhang 2009).

Hadronic models for explaining the gamma-ray emission of active galactic nuclei (AGNs) were also proposed. These models usually require a jet power larger than the Eddington luminosity by 1–2 orders of magnitude (e.g., Böttcher et al. 2013). Although a moderate proton power could be enough to model the

[4] TeVCat official website: http://tevcat.uchicago.edu/.

MeV–GeV bump of the SEDs (e.g., Cerruti et al. 2015), an extremely large jet power, which is larger than the Eddington luminosity by 4–5 orders of magnitude, is required to attribute the TeV excess to the contributions of the $p\gamma$ process (Cao & Wang 2014). This clarifies the issue of the breaking Eddington limit. Despite the Eddington luminosity not being a strict limit, it is a reasonable approximation for the maximum jet power of a blazar (e.g., Zdziarski & Bottcher 2015).

The observed TeV excess indicates that the $e^{\pm}$ pair production and its cascade emission within the jet may play a key role in shaping the observed SED in the keV–GeV band (Cerruti et al. 2015; Xue et al. 2021). More importantly, the cascade emission should offer an extra photon field for enhancing the very-high-energy (VHE) gamma-ray emission via the pγ process, leading to a reduction of the proton power that may relieve the tension of exceeding the Eddington luminosity to some extent. This Letter aims to explore the hadronic origin of the TeV excesses in the framework of the single-zone leptohadronic model by considering radiations of the relativistic electrons and protons together with their cascade process in detail. We present the selected broadband SEDs in Section 2, and describe our model in Section 3. The results are reported in Section 4. Our conclusion and discussion are given in Section 6. Throughout the paper, cosmological parameters of $H_0 = 70\,\mathrm{km\,s^{-1}\,Mpc^{-1}}$, $\Omega_\mathrm{m} = 0.3$, and $\Omega_\Lambda = 0.7$ are adopted.

2. Intrinsic TeV Excess in Selected SEDs of BL Lacs

We select some BL Lacs with clear detections of a TeV excess component over the leptonic model prediction in their SEDs. They are taken from Zhang et al. (2012) in which a large SED sample of 24 TeV BL Lacs is compiled and represented with the single-zone leptonic model. We derive the intrinsic SEDs by correcting the EBL absorption with the model in Finke et al. (2010).[5] Based on the leptonic model results presented in Zhang et al. (2012), we finally select the following 4 BL Lacs that have a TeV excess component over the leptonic model prediction with a confidence level of 3σ at the energy band of >0.1 TeV. The σ value is estimated as $\sigma = \sum_\mathrm{i}(|F_\mathrm{int,i} - F_\mathrm{t,i}|/\sigma_\mathrm{i})$, where $F_\mathrm{int,i}$ and σ_i are the intrinsic flux and its uncertainty, respectively, and $F_\mathrm{t,i}$ is the intrinsic flux predicted by the leptonic model. The selected SEDs for the 4 BL Lacs are shown in Figure 1 and described as follows.

1. *1ES 0229+200* ($z = 0.14$; Aharonian et al. 2000). This BL Lac is known for its hard spectrum in the TeV band. HESS observations of this source in 2005 and 2006 show a photon spectral index of ∼2.5 in the energy range 500 GeV to ∼15 TeV, yielding a very hard intrinsic spectrum at VHE band (Aharonian et al. 2007b). Between 2009 October and 2013 January, VERITAS detected an excess of 489 γ-ray events from 1ES 0229+200 in the energy range of 0.29–7.6 TeV, with an average integral flux of $\sim 23.3 \times 10^{-9}$ photons $\mathrm{m^{-2}\,s^{-1}}$(Aliu et al. 2014). The long-term observations of MAGIC, with a total of 265 hr good-quality data from 2010 to 2017, suggested that the intrinsic spectral index of 1ES 0229+200 is ∼1.8 at 521 GeV (Acciari et al. 2020), for which the EBL model of Franceschini et al. (2008) is considered. The hadronic origin of the VERITAS observation has been discussed with various models, for example, the proton–synchrotron and the leptohadronic models (Cerruti et al. 2015). In our work, multi-band data include VHE and X-ray observations, which are collected from Aharonian et al. (2007b) and Zhang et al. (2012), respectively.
2. *1ES 0347–121* ($z = 0.188$; Woo et al. 2005). This object was observed by HESS between 2006 August and December in the VHE band. The detected photon spectral index is ∼3.10 in the energy range 0.25–3 TeV, with an integral flux ∼2% of that of the Crab Nebula (Aharonian et al. 2007c). The hadronic origin of this VHE observation has also been studied and discussed (Cerruti et al. 2015). The multi-band data used in our intrinsic broadband SED analysis are obtained from Aharonian et al. (2007c), which includes ATOM and SWIFT observations.
3. *1ES 1101–232* ($z = 0.186$; Wolter et al. 2000). From 2004 March to 2005 June, HESS detected 1ES 1101–232 with an excess of 649 photons. This VHE observation shows a very hard intrinsic spectrum with a photon index ∼1.5 from 0.23 to 4 TeV (Aharonian et al. 2007a). Previous studies have indicated that the VHE emission may originate from the hadronic processes (e.g., Cao & Wang 2014; Cerruti et al. 2015). In this work, the multi-band data of the broadband SED including the HESS observation as well as the semi-simultaneous X-ray observation of XMM-Newton and RXTE taken from Costamante (2007).
4. *H2356–309* ($z = 0.165$; Bersanelli et al. 1992). The VHE observations of H2356–309 have been reported twice by HESS. The first one was from 2004 June to December with a photon index ∼3.09 in the energy range from 0.2 to 1.3 TeV (Aharonian et al. 2007d). The second one was observed over a long-term period, from 2004 to 2007, yielding an integral flux $\sim 3.06 \times 10^{-12}$ photons $\mathrm{cm^{-2}\,s^{-1}}$ above 240 GeV and a photon index ∼3.06 in the energy range from 200 GeV to 2 TeV (HESS Collaboration et al. 2010). It has been found that the H2356–309 location of the former is coincident with the error circles of three IceCube events, and the VHE emission may be from hadronic processes (Sahu & Miranda 2015). The multi-band data used in this paper were obtained from HESS Collaboration et al. (2010), incorporating the simultaneous optical/UV and X-ray observations from XMM-Newton, the NRT radio observation, and the ATOM optical observation.

3. Model

We employ a single-zone leptohadronic model to explain the broadband SEDs of the selected BL Lacs. The bimodal SEDs from the radio to the MeV–GeV γ-ray band are attributed to synchrotron radiation of electrons accelerated in the jet. The TeV excess is explained as the production of the interaction between accelerated protons and photons (pγ process). Cascade emission is considered following that presented by Böttcher et al. (2013). The injected cascade electrons include electrons produced via the internal $\gamma\gamma$ absorption for photon fields of both the leptonic and hadronic processes, and electrons from charged pion decay in the $p\gamma$ process (e.g., Atoyan & Dermer 2003; Romero & Vila 2008) as well as electrons resulting from the Bethe–Heitler process (e.g., Chodorowski et al. 1992; Kelner & Aharonian 2008). We describe the model in the following.

[5] The EBL model by Franceschini et al. (2008) is also adopted to double check the EBL corrections in our analysis. The difference of the derived intrinsic spectra induced by the two EBL models is not significant.

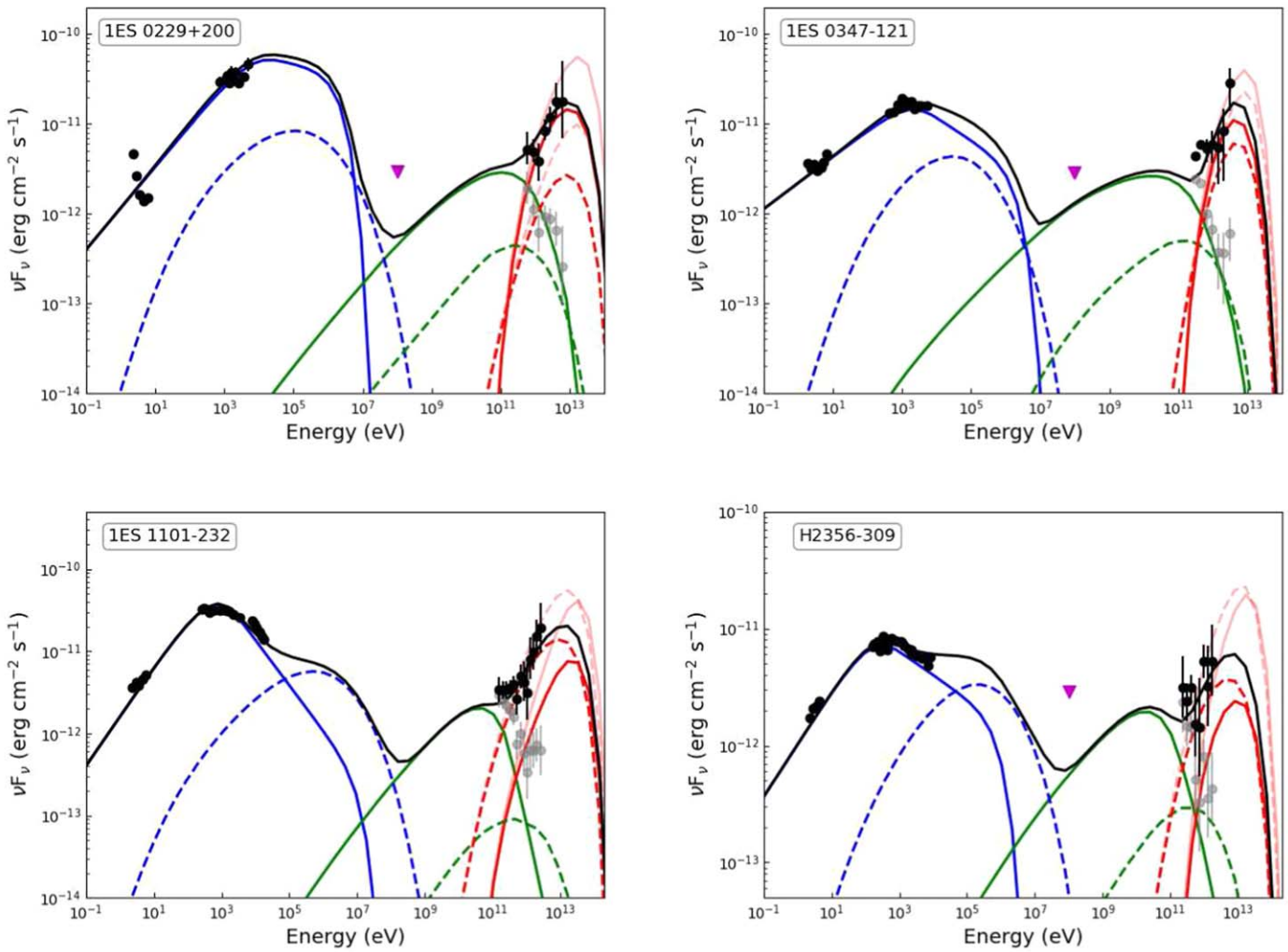

Figure 1. The EBL absorption-corrected SEDs (solid black dots with error bars) and our leptohadronic model results (solid black curves). The gray points are the observed data without the EBL absorption correction. The purple inverted triangles indicate the upper limit of the Fermi/LAT observations from Tavecchio et al. (2010). Color lines represent the different radiation processes: blue for synchrotron, green for SSC, and red for π^0 decay. Solid lines are for the emission of the primary electrons and dashed lines are for the emission of the cascade electrons. The hadronic emission without considering the internal $\gamma\gamma$ absorption are also drawn with red translucent solid/dashed lines for demonstration.

3.1. The Leptonic Radiation

We adopt the leptonic model of Zhang et al. (2012). The emitting region is assumed to be a single-zone sphere with a radius $R_{\rm b}$ moving with a bulk Lorentz factor Γ (or a velocity in units of light speed, β). $R_{\rm b}$ can be estimated with the minimum variability timescale, $R_{\rm b} = c\delta_{\rm D}\Delta t/(1+z)$, where $\delta_D = 1/\Gamma(1-\beta\cos\theta)$ is the Doppler factor with a viewing angle of θ to the jet axis. For BL Lacs, the jet orientation is close to the line of sight, and thus $\delta_{\rm D} \sim \Gamma$. The primary electron spectrum is taken as a broken power-law function with indices p_1 and p_2 breaking at $\gamma_{\rm e,b}$ in the range of $[\gamma_{\rm e,min}, \gamma_{\rm e,max}]$.

The bimodal SED feature in the radio–optical–X-ray–GeV–γ-ray band is attributed to synchrotron radiation and the SSC process of relativistic electrons. Our calculation of the synchrotron process is based on an approximation method (Aharonian et al. 2010), for which the synchrotron self-absorption (Katarzyński et al. 2001) is considered. The SSC process is calculated with analytical approximations (Khangulyan et al. 2014). The internal $\gamma\gamma$ absorption (Finke et al. 2008) is yielded, where the high-energy and low-energy photons are from SSC and synchrotron radiation, respectively. The radiative cooling of electrons can be estimated by the energy density of the magnetic field and the synchrotron photon field, in which the Klein–Nishina effect is incorporated (Moderski et al. 2005).

3.2. The Hadronic Radiation

We consider only the radiative cooling of the protons via the $p\gamma$ process. There are two main channels of this process: (1) the Bethe–Heitler (B–H) process, $\mathrm{p}+\gamma \rightarrow \mathrm{p}+\mathrm{e}^-+\mathrm{e}^+$ for photons with a threshold energy of $\sim$1 MeV in the proton rest frame (Kelner & Aharonian 2008) and (2) the photomeson process of single-pion pass $\mathrm{p}+\gamma \rightarrow \mathrm{p}+\mathrm{a}\pi^0+\mathrm{b}(\pi^+ + \pi^-)$ and multi-pion pass $\mathrm{p}+\gamma \rightarrow \mathrm{n}+\pi^+ + \mathrm{a}\pi^0 + \mathrm{b}(\pi^+ + \pi^-)$ (Romero & Vila 2008) for photons with a threshold energy of $\sim$145 MeV in the proton rest frame (Atoyan & Dermer 2003). A π^0 particle decays to two energetic photons, which may result in the observed TeV excess. The electrons generated through the two channels may be cooled via synchrotron radiation and the SSC process. This electromagnetic cascade emission may modify the SED in the radio–optical–X-ray–GeV band.

Our calculations of the $p\gamma$ process are based on the semi-analytical method under the framework of Atoyan & Dermer (2003) and Romero & Vila (2008). The collision rate of a proton with the Lorentz factor $\gamma_{\rm p}$ through the $p\gamma$ process with a soft photon field can be expressed as

$$\omega_{\rm p\gamma,i}(\gamma_{\rm p}) = \frac{c}{2\gamma_{\rm p}^2}\int_{\frac{\epsilon'_{\rm th,i}}{2\gamma_p}}^{\infty} d\epsilon \frac{n_{\rm ph}(\epsilon)}{\epsilon^2}\int_{\epsilon'_{\rm th,i}}^{2\epsilon\gamma_{\rm p}} d\epsilon'\sigma_{\rm p\gamma,i}(\epsilon')\epsilon', \quad (1)$$

where the subscript $\rm i = e,\ \pi$ represents for the B–H and photomeson processes respectively, $n_{\rm ph}(\epsilon)$ is the number density of photons with energy ϵ (the synchrotron radiation of electrons in our case), ϵ' and $\epsilon'_{\rm th,i}$ are the photon energy and photon threshold energy in the proton rest frame, and $\sigma_{\rm p\gamma,i}$ is the cross section. Thus, the cooling rate can be given by

$$\tau^{-1}_{\rm p\gamma,i}(\gamma_{\rm p}) = \frac{c}{2\gamma_{\rm p}^2}\int_{\frac{\epsilon'_{\rm th,i}}{2\gamma_p}}^{\infty} d\epsilon \frac{n_{\rm ph}(\epsilon)}{\epsilon^2} \int_{\epsilon'_{\rm th,i}}^{2\epsilon\gamma_{\rm p}} d\epsilon'\sigma_{\rm p\gamma,i}(\epsilon')K_{\rm p\gamma,i}(\epsilon')\epsilon', \quad (2)$$

where $K_{\rm p\gamma,e}$ is the inelasticity factor. The cross section $\sigma_{\rm p\gamma,e}$ and inelasticity $K_{\rm p\gamma,e}$ can be found in Chodorowski et al. (1992). For the photomeson process, the cross section and inelasticity can be approximated as

$$\sigma_{\rm p\gamma,\pi}(\epsilon') \approx \begin{cases} 3.4\times10^{-28}\,{\rm cm^{-2}}, & 200\,{\rm MeV} \leqslant \epsilon' \leqslant 500\,{\rm MeV} \\ 1.2\times10^{-28}\,{\rm cm^{-2}}, & \epsilon' > 500\,{\rm MeV}, \end{cases} \quad (3)$$

$$K_{\rm p\gamma,\pi}(\epsilon') \approx \begin{cases} 0.2, & 200\,{\rm MeV} \leqslant \epsilon' \leqslant 500\,{\rm MeV} \\ 0.6, & \epsilon' > 500\,{\rm MeV}, \end{cases} \quad (4)$$

in which the two energy ranges correspond to single-pion and multi-pion channels, respectively.

The proton distribution in the energy range $[E_{\rm p,min}, E_{\rm p,max}]$ is assumed to be an exponential cutoff power law with an index α and a cutoff energy $E_{\rm p,cut}$, i.e.,

$$N_{\rm p}(E_{\rm p}) = N_0\left(\frac{E_{\rm p}}{1\,{\rm eV}}\right)^{-\alpha}\exp\left(-\frac{E_{\rm p}}{E_{\rm p,cut}}\right), \quad E_{\rm p,min} \leqslant E_{\rm p} \leqslant E_{\rm p,max}. \quad (5)$$

The electron energy produced in the B–H process depends on the proton energy as $E_{\rm e} = \frac{1}{2}\overline{K}_{\rm p\gamma,e}E_{\rm p}$, and its productivity is

$$Q_{\rm BH,e}(E_{\rm e}) = \frac{4}{\overline{K}_{\rm p\gamma,e}}N_{\rm p}\left(\frac{2}{\overline{K}_{\rm p\gamma,e}}, E_{\rm e}\right)\omega_{\rm p\gamma,e}\left(\frac{2}{\overline{K}_{\rm p\gamma,e}}, \frac{E_{\rm e}}{m_{\rm p}c^2}\right). \quad (6)$$

The mean inelasticity $\overline{K}_{\rm p\gamma,e}$ can be approximated to $2m_{\rm e}/m_{\rm p}$ (Romero & Vila 2008). Because electrons produced through a single proton–photon interaction in the B–H process have a broad energy distribution, the productivity calculated through the mean inelasticity and Equation (6) is not accurate enough. Hence, we adopt an analytic method introduced by Kelner & Aharonian (2008) to calculate the electron production. This method is based on the differential cross section of the process and can provide better accuracy.

Mesons (π^0 and $\pi^{\pm}$) produced in the $p\gamma$ interaction would inherit about 20% of the energy from the collided proton and further pass it to photons and electrons, $E_\gamma \approx 0.1E_{\rm p}$ and $E_{\rm e} \approx 0.05E_{\rm p}$. The photon emissivity from π^0 decay and the electron emissivity from $\pi^{\pm}$ decay can be calculated as

$$Q_{p\gamma,\gamma}(E_\gamma) = 20N_{\rm p}(10E_\gamma)\omega_{\rm p\gamma,\pi}(10E_\gamma)n_{\pi^0}(10E_\gamma), \quad (7)$$

$$Q_{\rm p\gamma,e}(E_{\rm e}) = 20N_{\rm p}(20E_{\rm e})\omega_{\rm p\gamma,\pi}(20E_{\rm e})n_{\pi^{\pm}}(20E_{\rm e}), \quad (8)$$

where $n_{\pi^0} \approx 0.5p_1 + p_2$ and $n_{\pi^{\pm}} \approx 0.5p_1 + 2p_2$ are defined as the mean number of π^0 and $\pi^{\pm}$ created per collision, respectively. p_1 is the possibility of the $p\gamma$ interaction through the single-pion pass and $p_2 = 1 - p_1$ is for the multi-pion pass. They can be derived by defining the mean inelasticity as

$$\overline{K}_{\rm p\gamma,\pi} = \tau^{-1}_{\rm p\gamma,\pi}\omega^{-1}_{\rm p\gamma,\pi} = 0.2p_1 + 0.6(1 - p_1). \quad (9)$$

The specific luminosity of the gamma-ray photons from the π^0 decay in the comoving frame is given by

$$L_{\rm E}(E_\gamma) = 4\pi E_\gamma Q_{\rm p\gamma,\gamma}(E_\gamma)V \times \frac{1 - e^{-\tau_{\gamma\gamma}}}{\tau_{\gamma\gamma}}, \quad (10)$$

where $V = 4\pi R_{\rm b}^3/3$ is the volume of the radiating region and $\tau_{\gamma\gamma}$ is the optical depth of the internal $\gamma\gamma$ interaction (Finke et al. 2008). Without considering the EBL absorption, the intrinsic specific flux in the observed frame is $F_{\rm E}(E_{\gamma,\rm obs}) = (1+z)\delta_{\rm D}^3 L_{\rm E}(E_\gamma)/4\pi D_{\rm L}^2$, where $E_{\gamma,\rm obs} = E_\gamma\delta_{\rm D}/(1+z)$, $D_{\rm L}$ is the luminosity distance.

3.3. The Cascade Process

Generally, the pair cascade process is initiated by the internal $\gamma\gamma$ interaction of existing photon fields inside the radiation region, creating a loop between electron generation, cooling, and escaping. The system eventually reaches a temporary equilibrium and returns a stationary secondary electron distribution. The cascade process is calculated in a time-independent method (Böttcher et al. 2013), and the Fokker–Planck equation is written as

$$\frac{\partial}{\partial\gamma_{\rm e}}(\dot{\gamma}_{\rm e}N_{\rm e}^{\rm cas}) = Q_{\rm e}(\gamma_{\rm e}) + \dot{N}_{\rm e}^{\gamma\gamma}(\gamma_{\rm e}) + \dot{N}_{\rm e}^{\rm esc}(\gamma_{\rm e}), \quad (11)$$

where $Q_{\rm e}$ is the sum of the B–H and photomeson electrons in the $p\gamma$ interaction, $\dot{N}_{\rm e}^{\gamma\gamma}$ is the electron injection from the internal $\gamma\gamma$ interaction, $\dot{N}_{\rm e}^{\rm esc}$ is the escape term, and $N_{\rm e}^{\rm cas}$ is the final electron distribution. The particle escape can be estimated as $\dot{N}_{\rm e}^{\rm esc}(\gamma_{\rm e}) = N_{\rm e}^{\rm cas}(\gamma_{\rm e})/t_{\rm esc}$, where $t_{\rm esc} = R_{\rm b}/c$. $\dot{N}_{\rm e}^{\gamma\gamma}(\gamma_{\rm e})$ is given by

$$\dot{N}_{\rm e}^{\gamma\gamma}(\gamma_{\rm e}) = f_{\rm abs}(\epsilon_1)(\dot{N}^0_{\epsilon_1} + \dot{N}^{\rm syn}_{\epsilon_1} + \dot{N}^{\rm SSC}_{\epsilon_1}) + f_{\rm abs}(\epsilon_2)(\dot{N}^0_{\epsilon_2} + \dot{N}^{\rm syn}_{\epsilon_2} + \dot{N}^{\rm SSC}_{\epsilon_2}), \quad (12)$$

where $\dot{N}^0$ is the initial γ-rays from the π^0 decay, $\dot{N}^{\rm syn}$ and $\dot{N}^{\rm SSC}$ are the synchrotron and SSC radiations of $N_{\rm e}^{\rm cas}$, ϵ_1 and ϵ_2 are the energies of photons to produce $\gamma_{\rm e}$ electrons via the pair production, and $f_{\rm abs}$ is the internal absorption coefficient. ϵ_1 and ϵ_2 are estimated as $\epsilon_1 = \gamma_{\rm e}/f_\gamma$ and $\epsilon_2 = \gamma_{\rm e}/(1 - f_\gamma)$, where f_γ is a energy fraction of the two photons, which is taken to be 0.9 following Böttcher et al. (2013).

4. Results

Assuming that the protons are accelerated by relativistic shocks via the Fermi acceleration mechanism, the energy spectral index of

Table 1
Leptohadronic Model Parameters

Source	z	δ_D	B (G)	Δt hr	$\gamma_{e,min}$	$\gamma_{e,b}$	p_1	p_2	$N_{0,e}$ (cm^{-3})	$E_{p,max}$ (eV)	$E_{p,cut}$ (eV)	$N_{0,p}$ (cm^{-3} eV^{-1})
1ES 0229+200	0.139[(1)]	8.4	0.48	24	2	3.9×10^5	2.08	3.16	1.3×10^3	1×10^{15}	2.8×10^{13}	1.5×10^{18}
1ES 0347–121	0.188[(2)]	11	0.65	12	100	1.4×10^5	2.42	3.5	8.2×10^4	1×10^{14}	8×10^{12}	4.8×10^{19}
1ES 1101–232	0.186[(3)]	12	1.05	12	5	6.5×10^4	1.8	4.1	85	5×10^{14}	2.4×10^{13}	2.2×10^{19}
H2356–309	0.165[(4)]	7.6	0.5	24	2	6.3×10^4	2.1	3.4	3.8×10^3	1×10^{15}	2.8×10^{13}	1.1×10^{19}
Mrk 421	0.031[(5)]	29	0.058	3	20	4.5×10^5	2.36	4.0	1.9×10^5	1×10^{15}	2.8×10^{13}	4.5×10^{19}

References. (1) Aharonian et al. (2000); (2) Woo et al. (2005); (3) Wolter et al. (2000); (4) Bersanelli et al. (1992); (5) Punch et al. (1992).

the proton distribution is fixed at $p_p = 2.2$ in our calculations. In the leptohadronic model, contributions from the following spectral components shape the SEDs, i.e., (1) the primary leptonic emission components, including the synchrotron and SSC emission components from the primary electron population, (2) the primary VHE γ-ray component from the pγ process via the π^0 decay, in which photons are from the primary synchrotron radiation, (3) the cascade leptonic component, including the synchrotron and SSC emission components from the cascade electrons produced via the internal $\gamma\gamma$ interaction and the $p\gamma$ interaction, and (4) the cascade VHE γ-ray component from the cascade pγ process, in which photons are from the cascade synchrotron radiation. Our numerical results are shown in Figure 1 and the model parameters are reported in Table 1. One can observe that the model well represents the data. The parameters of the leptonic model part are generally consistent with those reported in the literature (e.g., Aharonian et al. 2007c; Costamante 2007; HESS Collaboration et al. 2010; Tavecchio et al. 2010; Zhang et al. 2012). The cutoff energy ($E_{p,cut}$) of protons is typically 10 TeV.

As shown in Figure 1, the synchrotron radiation of the primary electron population overwhelmingly dominates the SEDs in the optical–soft-X-ray band ($1 \sim 10^4$ eV), and the SSC components of the primary electron population peak at around 10 GeV for the four BL Lacs. The cascade synchrotron radiation bump peaks at around 0.1 MeV. The peak fluxes of both the synchrotron radiation and the SSC emission components of the cascade electron population are lower than that of the primary electron population by a factor of $2 \sim 10$. The combinations of the primary and cascade synchrotron emission components shape the SEDs as a distinct hump or a plateau in the keV–MeV energy band, as shown in the SEDs of 1ES 0347–121, 1ES 1101–232, and H2356–309. Such a keV–MeV excess would be a distinct feature of the hadronic process.

The TeV γ-rays are contributed by the π^0 decay process in the primary (or cascade) pγ interactions, in which the soft γ-ray photon fields are the synchrotron radiation of the primary (or cascade) electron population. Both the primary and cascade SSC emission decrease rapidly at high energies because of the Klein–Nishina effect, making negligible contributions to the TeV excess. The π^0 decay process completely dominates the TeV γ-ray flux, although the internal $e^{\pm}$-pair production is very significant for these VHE γ-ray photons. Since we have fixed the energy spectral index of the injected proton distribution, the shape of the hadronic spectrum depends largely on the soft photon fields. Note that the photon threshold energy of the pγ interaction is $\epsilon_{th} > 145\,\mathrm{MeV}/2\gamma_p$. Thus, the soft photons should be at least as energetic as 10 keV for generating the TeV γ-rays. For 1ES 0229+200 and 1ES 0347–121, the peak flux of the TeV γ-rays from the primary pγ interactions is larger than that from the cascade pγ interactions. Inversely, the TeV γ-ray peak flux in 1ES 1101–232 and H2356–309 is mainly contributed by the cascade pγ interactions. The intrinsic total peak flux of the TeV excess is $F_{int,p} \sim 1 \times 10^{-11}$ erg cm^{-2} s^{-1}, comparable to the synchrotron peak flux of the primary electrons.

5. Discussion

5.1. The Issue of Breaking Eddington Limit

The derived jet power breaking the Eddington luminosity limit is a long-standing issue in single-zone hadronic (leptohadronic) models (e.g., Böttcher et al. 2013). This issue is clarified while explaining the TeV excess with gamma-rays generated through the pγ process (Cao & Wang 2014) due to inefficient radiative cooling of the protons. We compare the cooling rates of protons and electrons in our model in Figure 2. It is found that the primary electrons with energy $<10^9 \sim 10^{10}$ eV are efficiently cooled via the SSC process, and the cooling of electrons with energy $\gtrsim 10^{10}$ eV is dominated by synchrotron radiation due to the Klein–Nishina effect reducing the cross section of high-energy electrons. The cooling rates of the protons in the energy range from 1 TeV to 100 TeV via the B–H and photomeson processes are about $10^{-15} \sim 10^{-12}$ s^{-1}. In most cases, the photomeson process is less efficient than the B–H process, which has a much lower threshold photon energy. However, the B–H process has a limited influence in calculating the cascade process for relatively small cross sections and inelasticity. Electron injections from the internal pair production and the charged pion decay are the major parts that decide the stationary electron distribution of the cascade process.

It was also proposed that the TeV excess results from the $p\gamma$ process with an extremely dense photon field (Sahu et al. 2013). However, how to form such a photon field is a great challenge in this model. In our analysis, the cascade synchrotron photon field is considered in the pγ process to enhance the production of VHE photons. We estimate the proton powers of the sources as $P_p = \pi R_b^2 \Gamma^2 c U_p$ with the parameters reported in Table 1. Our results are $P_p = 2.19 \times 10^{50}$, 4.31×10^{51}, 3.06×10^{51}, and 9.85×10^{50} erg s^{-1} for 1ES 0229+200, 1ES 0347–121, 1ES 1101–232, and H2356–309, and their Eddington luminosities are 2.19×10^{47}, 5.63×10^{46}, 1.26×10^{47}, and 5.02×10^{46} erg s^{-1}, respectively.[6] Note that the derived proton powers in our model are lower than that without considering the cascade synchrotron photon field by one order of magnitude, i.e., 3.06×10^{51} versus

[6] Since no estimated central black hole mass of 1ES 1101–232 is available, we use an average black hold mass $10^9 M_\odot$ instead.

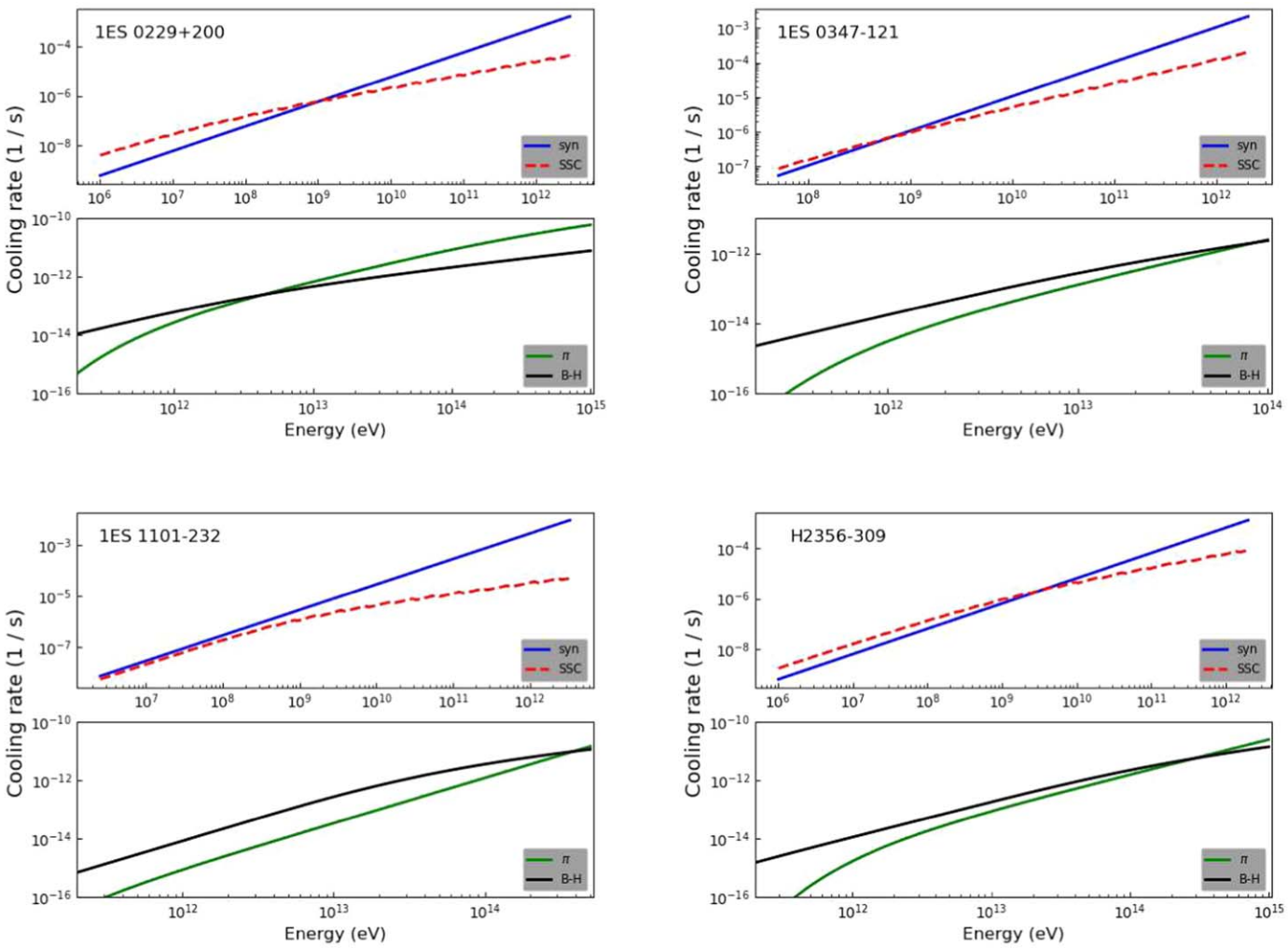

Figure 2. The cooling rates of the primary synchrotron and SSC as well as the primary pγ components. The upper panel and the lower panel are the cooling rates of the primary electrons and protons for the 4 BL Lacs.

3.10×10^{52} erg s^{-1} of 1ES 1101–232 for instance. However, they are still 3–4 orders of magnitude larger than the Eddington luminosities.

5.2. Magnetic Field Strength and Proton Acceleration

In our leptohadronic model, the magnetic field strength is about $0.1 \sim 1$ G, comparable to that used in leptonic models for explaining the SEDs below the TeV band, but 2–3 orders of magnitude smaller than that required in the proton–synchrotron hadronic model for representing the MeV–GeV gamma-ray bump (e.g., Böttcher et al. 2013; Cerruti et al. 2015). We examine whether the proton can be sufficiently accelerated under the relatively small magnetic field strength. Assuming $B = 0.5$ G, the Larmor radius of a 100 TeV proton is $\sim 6.67 \times 10^{11}$ cm, which is still smaller than the typical emitting region size by 5–6 orders of magnitude. Therefore, the magnetic field strength used in our model should be sufficient to accelerate the proton to relativistic in the radiating region.

The particle acceleration mechanism in BL Lacs is still uncertain. In our analysis, we assume that the charged particles are accelerated by the Fermi acceleration mechanism via relativistic shocks, and the proton distribution $N_{\rm p}(E_{\rm p}) \propto E_{\rm p}^{-2.2}$ is adopted. Note that particles accelerated through magnetic reconnection may result in a harder particle distribution (e.g., Zhu et al. 2016 and references therein). The number density of the low-energy end of the proton distribution can be significantly reduced, leading to a decrease of the required proton power in our model. We test this scenario with 1ES 1101–232 by taking the proton distribution index as -1.5. The SED is still well represented, and the derived P_p is reduced by a factor of 4.5, changing from 3.06×10^{51} to 6.96×10^{50} erg s^{-1}. Meanwhile, narrowing the energy range, i.e., setting a larger $E_{\rm p,min}$, for the proton distribution can also help to reduce the power. The $E_{\rm p,min}$ value is fixed at 10 GeV in our calculations for the 4 BL Lacs. By setting $E_{\rm p,min} = 100$ GeV, the derived proton power changes from 3.06×10^{51} to 1.58×10^{51} erg s^{-1} for 1ES 1101–232. Unfortunately, neither of the approaches we have tested can lower the jet power to an acceptable level concerning the Eddington luminosity that the supper-Eddington issue still exists.

5.3. Synergy of the TeV excess and keV–MeV excess as a probe for the hadronic process

Our analysis shows that the flux of the cascade synchrotron emission peaks at the keV–MeV energy band. Since it is usually lower than the primary synchrotron flux in the keV band, it may be featured as a keV–MeV excess (a bump or plateau) in the observed SEDs. The TeV excess and the

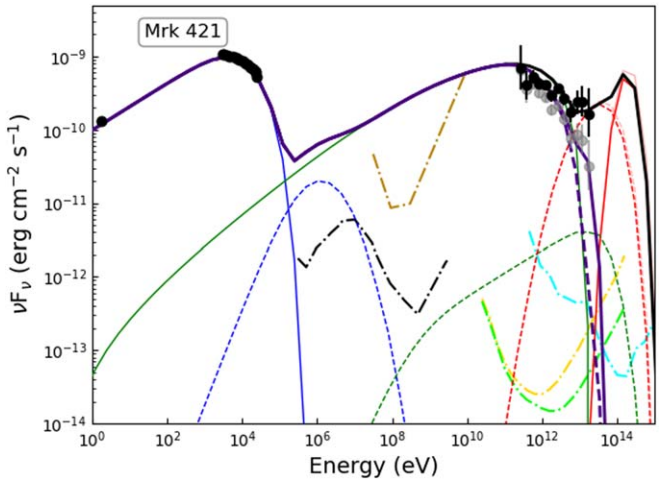

Figure 3. Intrinsic (black dots) and observed (gray dots) SEDs of Mrk 421 and our theoretical modeling (showing with the same symbols as that in Figure 1) together with examination of detection capability with some instruments for the TeV and MeV excesses in the TeV and MeV bands (showing with the same symbols as that in Figure 4).

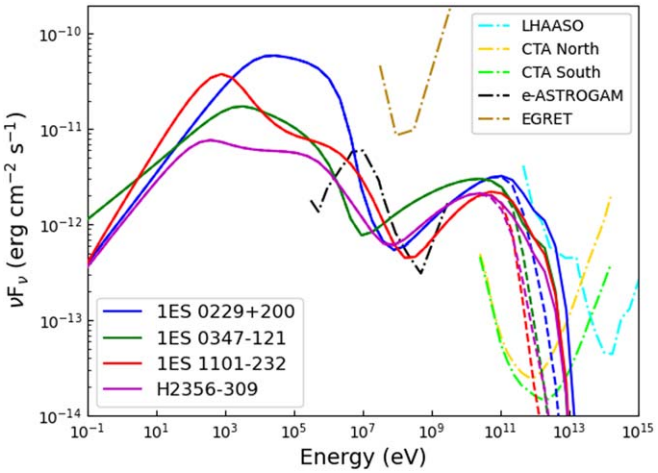

Figure 4. Examination of the detection capability of some instruments for the TeV and MeV excesses in the TeV and MeV bands. The solid lines are our model results presented in Figure 1 by considering the EBL absorption. The dashed lines mark the EBL-absorbed SSC component of the primary electron population. The one-year sensitivities of the instruments are plotted with dashed–dotted lines in different colors as marked in the plot.

corresponding keV–MeV excess would be promising probes for the hadronic process. Nearby Mrk 421 ($z = 0.031$; Punch et al. 1992) is the best candidate to verify this speculation. So far, Mrk 421 has been detected in the TeV band by the HESS, VERITAS, ARGO-YBJ, and MAGIC telescopes. It was detected during 2003–2004 with an outburst of a peak flux $\sim$135 mCrab in the X-ray band and $\sim$3 Crab in the γ-ray band (Błażejowski et al. 2005). A tentative TeV excess with large error bars is presented in its SED, as shown in Figure 3. The possible hadronic explanation of the VHE observations has already been discussed (e.g., Mastichiadis et al. 2013; Zech et al. 2017). Here we represent the SED with our leptohadronic model, and the result is also shown in Figure 3. As with the other four BL Lacs, the TeV excess of Mrk 421 is mainly contributed by π^0 decay. Interestingly, Nandikotkur et al. (2008) reported an intriguing convex break at 235 MeV in the SED of Mrk 421 observed with CGRO/EGRET. It is possible that the keV–MeV excess moves in the EGRET energy band during the EGRET observation campaign, shaping the convex break.

A great opportunity for testing our speculation is available with the current and upcoming VHE telescopes. The Large High Altitude Air Shower Observatory (LHAASO, Bai et al. 2019) is sensitive in the 0.1 TeV–1 PeV energy band, and the upcoming Cherenkov Telescope Array (CTA, Actis et al. 2011) is sensitive in the 20 GeV–300 TeV energy band.[7] Their synergy observations provide an unprecedented chance to investigate the particle acceleration and radiation physics of TeV–PeV γ-rays. We show the detectability of the TeV excess in the SEDs for the four BL Lacs with LHAASO and CTA in Figure 4, where one-year sensitivities are used. One can find that the TeV excess is not clearly shown in the observed SEDs due to the strong EBL absorption effect, which usually flattens the observed spectrum above the 0.1 TeV range. In contrast, it should be confidently detectable with the CTA up to $\sim$10 TeV for the four BL Lacs. The TeV excess in 1ES 0229+200 may also be marginally detectable with the LHAASO in the energy range of several TeV. Meanwhile, The TeV excess of Mrk 421 predicted by our model is detectable with the CTA and LHAASO up to $\sim$40 TeV. Its spectrum in the $8 \sim 17$ TeV energy band is predicted as $F_\nu \propto \nu^{-1.8}$. We have proposed to verify this TeV excess using the first operation year data of the LHAASO.

The keV–MeV excesses of the four BL Lacs are around $0.1 \sim 10$ MeV. Although they are marginally in the energy range of the EGRET ($0.2 \sim 100$ MeV; Hartman et al. 1999), it is not sensitive enough for the detection. However, the keV–MeV excess of H2356–309 was tentatively observed in the X-ray band, showing up like an X-ray plateau with a distinct feature of spectral hardening. Missions have been proposed for observations on the MeV γ-rays that have sensitivities higher than current/past missions by one or two orders of magnitude. For instance, the e-ASTROGAM is designed to improve the instrument sensitivity in the energy range of $0.3 \sim 100$ MeV with one-year sensitivity of $\sim 1.3 \times 10^{-12}$ erg cm^{-2} s^{-1} at $\sim$0.5 MeV (de Angelis et al. 2018). As shown in Figure 4, the keV–MeV excess should be detectable with the e-ASTROGAM.

6. Summary

We have investigated the hadronic origin of the observed TeV excess for four selected TeV BL Lacs (1ES 0229+200, 1ES 0347–121, 1ES 1101–232, and H2356–309) with a single-zone leptohadronic model by considering the cascade emission within their jets in detail. We summarize our results as follows.

1. Their broadband SEDs are well represented by our model. The SED in the radio–optical–X-ray–GeV gamma-ray energy band is mainly attributed to the synchrotron radiations and the SSC process of the primary electron population. The model parameters are consistent with those in leptonic models. The TeV excess is explained with the VHE γ-ray emission from the pγ process via the π^0 decay, assuming that the power-law index of the proton distribution is -2.2. The target photon fields are from the synchrotron radiations of the primary electron population and the cascade electron population produced via the internal $\gamma\gamma$ absorption and the pγ process.

[7] CTA official website: https://www.cta-observatory.org/.

2. The cascade synchrotron radiations result in an excess in the keV–MeV band of the SEDs, illustrated as a distinct bump or plateau as shown in the SEDs of 1ES 0347–121, 1ES 1101–232, and H2356–309. The keV–MeV excess enhances the production of VHE photons in the $p\gamma$ process and reduces the proton power by about one order of magnitude. However, the derived powers are still 3–4 orders of magnitude larger than the Eddington luminosity. Further tests by setting the power-law index of the proton energy distribution as -1.5 and enlarging the low energy boundary of the proton energy distribution, the derived proton power is reduced by a factor around 2–4. The breaking Eddington limit issue is still cannot be overcome. Thus, our model is challenged by the current accretion picture of AGNs.
3. Tentative TeV excess and MeV excess were observed in nearby bright TeV source Mrk 421. As predicted by our model, its TeV excess is mainly contributed by the cascade pγ emission, which dominates the observed SED beyond 5 TeV and can be detectable with the CTA and LHAASO up to ∼40 TeV. The convex break at 235 MeV in the SED of Mrk 421 observed with the EGRET might be resulted from its MeV excess. Mrk 421 is the best candidate for testing our model by synergic observations of the TeV excess and keV–MeV excess with LHAASO, CTA, and future missions that are sensitive in the keV–MeV energy band.

We thank Jin Zhang, Xiang Yu Wang, Ruo Yu Liu, and Rui Xue for help discussion. We also thank Jin Zhang for providing us with the SED data. This work is supported by the National Natural Science Foundation of China (grant No.12133003 and U1731239), Guangxi Science Foundation (grant No. 2017AD22006) and Innovation Project of Guangxi Graduate Education (YCBZ2021025).

ORCID iDs

Ji-Gui Cheng https://orcid.org/0000-0002-2585-442X
En-Wei Liang https://orcid.org/0000-0002-7044-733X

References

Acciari, V. A., Ansoldi, S., Antonelli, L. A., et al. 2020, ApJS, 247, 16
Actis, M., Agnetta, G., Aharonian, F., et al. 2011, ExA, 32, 193
Aharonian, F., Akhperjanian, A. G., Barres de Almeida, U., et al. 2007b, A&A, 475, L9
Aharonian, F., Akhperjanian, A. G., Barres de Almeida, U., et al. 2007c, A&A, 473, L25
Aharonian, F., Akhperjanian, A. G., Barres de Almeida, U., et al. 2007d, A&A, 475, L9
Aharonian, F., Akhperjanian, A. G., Bazer-Bachi, A. R., et al. 2007a, A&A, 470, 475
Aharonian, F. A., Akhperjanian, A. G., Barrio, J. A., et al. 2000, A&A, 353, 847
Aharonian, F. A., Kelner, S. R., & Prosekin, A. Y. 2010, PhRvD, 82, 043002
Aliu, E., Archambault, S., Arlen, T., et al. 2014, ApJ, 782, 13
Atoyan, A. M., & Dermer, C. D. 2003, ApJ, 586, 79
Bai, X., Bi, B. Y., Bi, X. J., et al. 2019, arXiv:1905.02773
Bersanelli, M., Bouchet, P., Falomo, R., & Tanzi, E. G. 1992, AJ, 104, 28
Błażejowski, M., Blaylock, G., Bond, I. H., et al. 2005, ApJ, 630, 130
Böttcher, M., Dermer, C. D., & Finke, J. D. 2008, ApJL, 679, L9
Böttcher, M., Reimer, A., Sweeney, K., & Prakash, A. 2013, ApJ, 768, 54
Cao, G., & Wang, J. 2014, ApJ, 783, 108
Cerruti, M., Zech, A., Boisson, C., & Inoue, S. 2015, MNRAS, 448, 910
Chodorowski, M. J., Zdziarski, A. A., & Sikora, M. 1992, ApJ, 400, 181
Costamante, L. 2007, Ap&SS, 309, 487
de Angelis, A., Tatischeff, V., Grenier, I. A., et al. 2018, JHEAp, 19, 1
Finke, J. D., Dermer, C. D., & Böttcher, M. 2008, ApJ, 686, 181
Finke, J. D., Razzaque, S., & Dermer, C. D. 2010, ApJ, 712, 238
Franceschini, A., Rodighiero, G., & Vaccari, M. 2008, A&A, 487, 837
Ghisellini, G., & Madau, P. 1996, MNRAS, 280, 67
Gould, R. J., & Schréder, G. 1966, PhRvL, 16, 252
Hartman, R. C., Bertsch, D. L., Bloom, S. D., et al. 1999, ApJS, 123, 79
HESS Collaboration, Abramowski, A., Acero, F., et al. 2010, A&A, 516, A56
Katarzyński, K., Sol, H., & Kus, A. 2001, A&A, 367, 809
Kelner, S. R., & Aharonian, F. A. 2008, PhRvD, 78, 034013
Khangulyan, D., Aharonian, F. A., & Kelner, S. R. 2014, ApJ, 783, 100
Mannheim, K. 1993, PhRvD, 48, 2408
Maraschi, L., Ghisellini, G., & Celotti, A. 1992, ApJL, 397, L5
Mastichiadis, A., Petropoulou, M., & Dimitrakoudis, S. 2013, MNRAS, 434, 2684
Moderski, R., Sikora, M., Coppi, P. S., & Aharonian, F. 2005, MNRAS, 363, 954
Nandikotkur, G., Jahoda, K. M., Georganopoulos, M., et al. 2008, preprint from NASA Technical Reports Server, https://ntrs.nasa.gov/citations/20080032432
Punch, M., Akerlof, C. W., Cawley, M. F., et al. 1992, Natur, 358, 477
Romero, G. E., & Vila, G. S. 2008, A&A, 485, 623
Sahu, S., & Miranda, L. S. 2015, EPJC, 75, 273
Sahu, S., Oliveros, A. F. O., & Sanabria, J. C. 2013, PhRvD, 87, 103015
Tavecchio, F., Ghisellini, G., Ghirlanda, G., Foschini, L., & Maraschi, L. 2010, MNRAS, 401, 1570
Urry, C. M., & Padovani, P. 1995, PASP, 107, 803
Wolter, A., Tavecchio, F., Caccianiga, A., Ghisellini, G., & Tagliaferri, G. 2000, A&A, 357, 429
Woo, J.-H., Urry, C. M., van der Marel, R. P., Lira, P., & Maza, J. 2005, ApJ, 631, 762
Xue, R., Liu, R.-Y., Wang, Z.-R., Ding, N., & Wang, X.-Y. 2021, ApJ, 906, 51
Yan, D., Zeng, H., & Zhang, L. 2012, MNRAS, 424, 2173
Zdziarski, A. A., & Bottcher, M. 2015, MNRAS, 450, L21
Zech, A., Cerruti, M., & Mazin, D. 2017, A&A, 602, A25
Zhang, J. 2009, RAA, 9, 777
Zhang, J., Liang, E.-W., Zhang, S.-N., & Bai, J. M. 2012, ApJ, 752, 157
Zhu, Y.-K., Zhang, J., Zhang, H.-M., et al. 2016, RAA, 16, 170